Journal of Porous Materials (2023) 30:1021–1036
https://doi.org/10.1007/s10934-022-01405-z

Effect of influencing parameters on developing aluminium metal foam by using powder metallurgy technique with a foaming agent as a wax powder

Mahadev Madgule[1] · **C. G. Sreenivasa**[2] · **Avinash V. Borgaonkar**[1]

Accepted: 25 November 2022 / Published online: 4 December 2022

Abstract
Aluminum metal foam has become an advanced popular material because it has excellent mechanical and electrical properties and is lightweight. The present work developed the Aluminium metal foam specimen using wax powder as a blowing agent through the powder metallurgy method. The effect of process parameters such as powder size, stirring speed, sintering temperature, and foaming agent content on the mechanical behavior of the developed specimens has been studied experimentally. In the design of experiments, the Taguchi orthogonal L9 array has been implemented. The percentage of porosity was estimated using the Archimedes principle, and mechanical behaviors such as flexural, tensile, and compressive strength were determined. The ANOVA analysis of variance it's been carried out to check the significant parameters affecting the mechanical behavior of developed specimens. It was observed that the powder size is the highly significant parameter, followed by stirring speed, the content of the foaming agent, and sintering temperature. The Maximum Porosity is 71.30%, Compression strength 12.01 MPa, Tensile strength is 6.16 MPa, and Flexural strength is 5.18 MPa. The microstructure study reveals that there is no adequate composition in the specimen. The novelty in this research work is using a novel foaming agent as a Wax powder to develop aluminium metal foam and attain good properties.

Keywords Aluminium metal foam · Wax powder · Powder metallurgy · Porosity · Mechanical properties · Taguchi

Abbreviations

AFs	Aluminium foams
AFM	Aluminium metal foam
CMFs	Composite metal foams
Ni	Nickel
Al	Aluminium
MMSFs	Metal matrix synthetic foams
DOE	Design of experiments
TiH_2	Titanium hydride
CNTs	Carbon nanotubes
$CaCO_3$	Calcium carbonate
H_2	Hydrogen
SiC	Silicon carbide
ISO	International organization for standardization
ASTM	American society for testing and materials
UTM	Universal testing machine
SEM	Scanning electron microscope
XRD	X-ray diffraction
S/N	Signal to noise
EDS	Energy dispersive X-ray spectroscopy

1 Introduction

Aluminum metal foam has been widely used in aerospace, automotive components, civil engineering, renewable energy field, and biomedical implants due to its lightweight and good mechanical properties [1, 2]. The metallic foam has a porous composite structure due to which it possesses excellent strength to weight, ideal thermal, sound, acoustic insulation, and superior impact energy absorption [3–5], heat insulation [6] electromagnetic shielding [7]. There are several techniques to produce metal foam ranging from liquid to solid route like direct foaming, space holder, ball making, and casting for the Aluminium metal foam. The powder metallurgy technique is the best process to achieve

✉ Mahadev Madgule
mahadev.madgule@gmail.com

[1] Department of Mechanical Engineering, Pimpri Chinchwad College of Engineering, Pune, Maharashtra 411044, India

[2] Department of Mechanical Engineering, UBDT College of Engineering, Davangere, Karnataka 577004, India

uniform pores structure over the specimen in the case of open or closed cells [8–10]. The high-temperature fabricated composite reveals the foam with a stable and homogeneous distribution. They investigated the effects of changes in structural characteristics of foam density on their mechanical properties. In another study, the Aluminium metal foams were developed through Aluminium powder Carbamide as a space holder route. They studied the effects of variation in the compressive behavior of Aluminium foam of relative density, size, and pore shape [11–13]. The fabrication techniques have their mechanical, thermal, and acoustic properties and potential applications [14–18].

The literature study shows that Bouwhuis et al. investigated the mechanical behavior, and failure analysis observed that electrodeposited nanocrystalline Ni reinforced in uniaxial compression of Aluminium metal foam. Ni foam with hollow nanocrystalline tube behavior is predicted in cellular composite material [19]. Brown et al. developed composite metal foams (CMFs) using water-cooled, air-casting, and powder metallurgy methods. The performance of developed CMFs was studied under a bending test during loading with in-situ acoustic emission analysis [20, 21]. The AFs were produced with different pore densities. The flexural strength and stiffness of the prepared samples were examined. The study's finding shows that composite was found to decrease in pore size with higher stiffness. The increase in the composites' stiffness was found with a decrease in pore size. The non-destructive and mechanical tests were performed to estimate the metal foams' properties [22] accurately. Kim et al. developed various mathematical correlations in AF's compressive properties and electrical conductivity [23]. Kadkhodapour and Raeisi investigated the relative density of mechanical behavior of closed porous cell AF using a numerical method. The obtained results were analyzed with analytical and experimental results [24]. Jung and Diebels reviewed the different micromechanical characterization techniques for metal foams and reported their usage in various applications [25]. Jung et al. developed a micro-tensile test setup for AF and hybrid Ni/Al foams to investigate the stress–strain curves [26, 27]. The test results reveal that different material behavior, such as hardening plastic behavior, young modulus, and fracture behavior, can be studied from the obtained stress and strain relationship. Duarte and Ferreira reported the various micro-size reinforcements to improve the mechanical behavior of open metal porous cells and closed metal porous cell Aluminium metal foams [28]. García et al. reviewed the different production processes of metal foams, their properties, and their commercial applications [17]. Orbulov and Szlancsik evaluated the mechanical behavior of metal matrix syntactic foams with the Aluminium matrix. In addition, fatigue properties and toughness of MMSFs have been assessed [29]. Shunmugasamy and Mansoor investigated the compressive behavior of open-cell 6101 AF in as-cast and as-rolled conditions [30]. Nawaz and Rani fabricated Aluminium alloy 6063 foam and evaluated their percent porosity and density using the Archimedes principle [31]. Liu et al. proposed a novel method for assessing the surface area of the metal foam porous region with mathematical co-relation between the porosity and pore diameter [32]. The developed mathematical model helps to predict the required data precisely. Aluminum metal foam's closed cell static behavior in shear and tension was studied to determine their mechanical behavior and failure analysis modes [33–37]. Ali et al. manufactured the hybrid closed-cell AF and investigated the effect of the different parameters, such as temperature and wt. % foaming agent and mixing speed on the porous area and pore size using the Taguchi DOE approach [38, 39]. The study shows that amount of the foaming agent is the highly significant factor, followed by stirring speed and temperature. In another study, the AFs were produced by the powder metallurgy method with Titanium hydride, TiH_2 as a foaming agent. A multi-objective optimization approach studied the effect of foaming agent content, compaction pressure, and temperature [40]. Arif et al. fabricated the aluminum foams reinforced with silicon carbide and carbon nanotubes using a powder metallurgy approach. The aluminum alloy in powder form was used as the matrix material, titanium hydride (TiH_2) powder was used as a foaming agent, and silicon carbide (SiC) particles and carbon nanotubes (CNTs) were used as reinforcing elements [41]. The test results show that the CNT and SiC particles significantly affected the elastic-plastic deformation behavior of the precursor materials. Further, Ding et al. reported a new method for optimizing the cellular structure of alloy foams by pretreating TiH_2 with a layer of powder. They observed that TiH_2 was completely encapsulated in the molten Sn at an early stage of foaming when the matrix alloy was still solid. This assists in capturing the liberated H_2 when TiH_2 begins to decompose. Eventually, this helps to avoid cracks in the solid matrix by enhancing the utilization ratio of TiH_2 as a blowing agent [42]. Geramipour and Oveisi [43] produced semi-open-cell aluminum foams with $CaCO_3$ as a foaming agent using a powder compact melting process. They studied the effects of various parameters such as precursor compaction pressure, foaming agent content, temperature, and time of the foaming process on the cell microstructure, linear expansion, relative density, and compressive properties of the foam. Anne Jung and Stefan Diebels [25] reported that the microstructure study of aluminum metal foams is separated into macro scale, meso scale, and micro-scale over the specimen with individual pores and struts, respectively. Macroscopic foam scales have stronger properties as compared to micro and meso scale it can be examined through computer tomography measurement for individual struts or cells. Tong Shi et al. [35] reported that the aluminum metal foam cell wall comprises an Al matrix

with Ca and Ti phases. The pore structure and cell wall are the major concerns with mechanical properties. The microstructure reveals that sophisticated cell walls will result in poor mechanical properties. When the pore structure is the same with different microstructure cell walls, it will affect microdeformation and directly affect the mechanical properties.different cell microstructure with thermal aging treatment shows that high energy absorption capacity. M. J. Mirzaali et al. [25] reported open and closed-cell aluminium metal foam with isotropic distribution cells along the length. The microstructural variation of pores can be examined through micro-CT imaging.

The literature study confirmed that Metal foam has broad applications, but it is still not used widely. The main challenging task is to achieve a good percentage of porosity in the prepared specimen with a uniform integrity structure over the entire sample. Paraffin Wax powder (C_nH_{2n+2}) foaming agent is used because during the powder metallurgy process, the porosity is developed as the H_2 liberated [36] paraffin wax powder has maximum hydrogen chemical composition content. Hence, in the present work, the aluminum metal foam is developed through a powder metallurgy approach using wax powder as a foaming agent to achieve good porosity and uniform structure. Taguchi's DOE approach is followed to investigate the effect of various input process parameters on the mechanical behavior of the developed AFM samples. Eventually, variance analysis (ANOVA) was implemented to know the significant and essential factors affecting output properties.

2 Materials and methods

2.1 Preparation of specimen of aluminium metal foam

The Aluminium Metal Foam (AMF) specimens were prepared with a powder metallurgy method. The detailed process parameters as shown in Fig. 1. The details process steps followed in the powder metallurgy process as shown in Fig. 2. The Aluminium (6061) was selected as the base powder and the wax as a foaming agent, as shown in Fig. 3a,

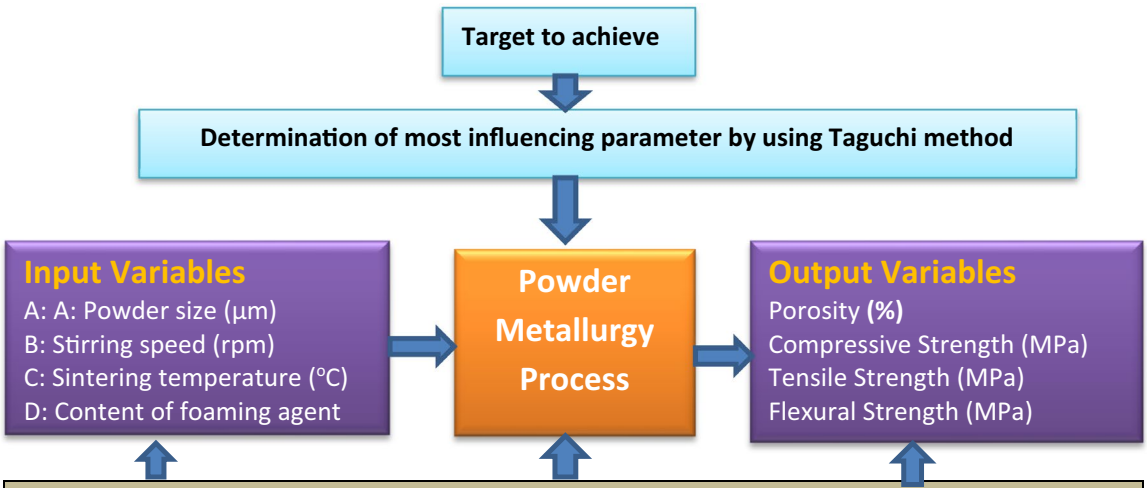

Parameters

Factors	Details	Factors	Details	Factors	Details
Powder size (µm)	100-140	Base material	Al 6061	Compressive specimen size (mm)	30mm Cube as per ISO 13314-2011
Stirring speed (rpm)	1000-1400	Foaming agent	Paraffin Wax	Tensile specimen size (mm)	200mm X25mmX12.5mm as per ASTM D3039
Sintering temperature (°C)	300-50	Compressive load in PM method (KN)	30	Flexural specimen size (mm)	110mmX30mmX10mm as per ASTM D790

Fig. 1 Process details of research work

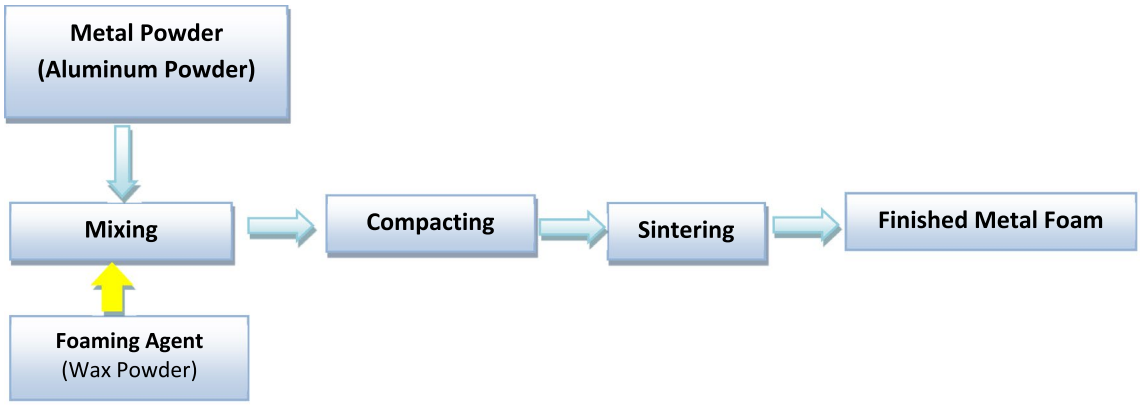

Fig. 2 Flowchart of foam preparation by powder metallurgy

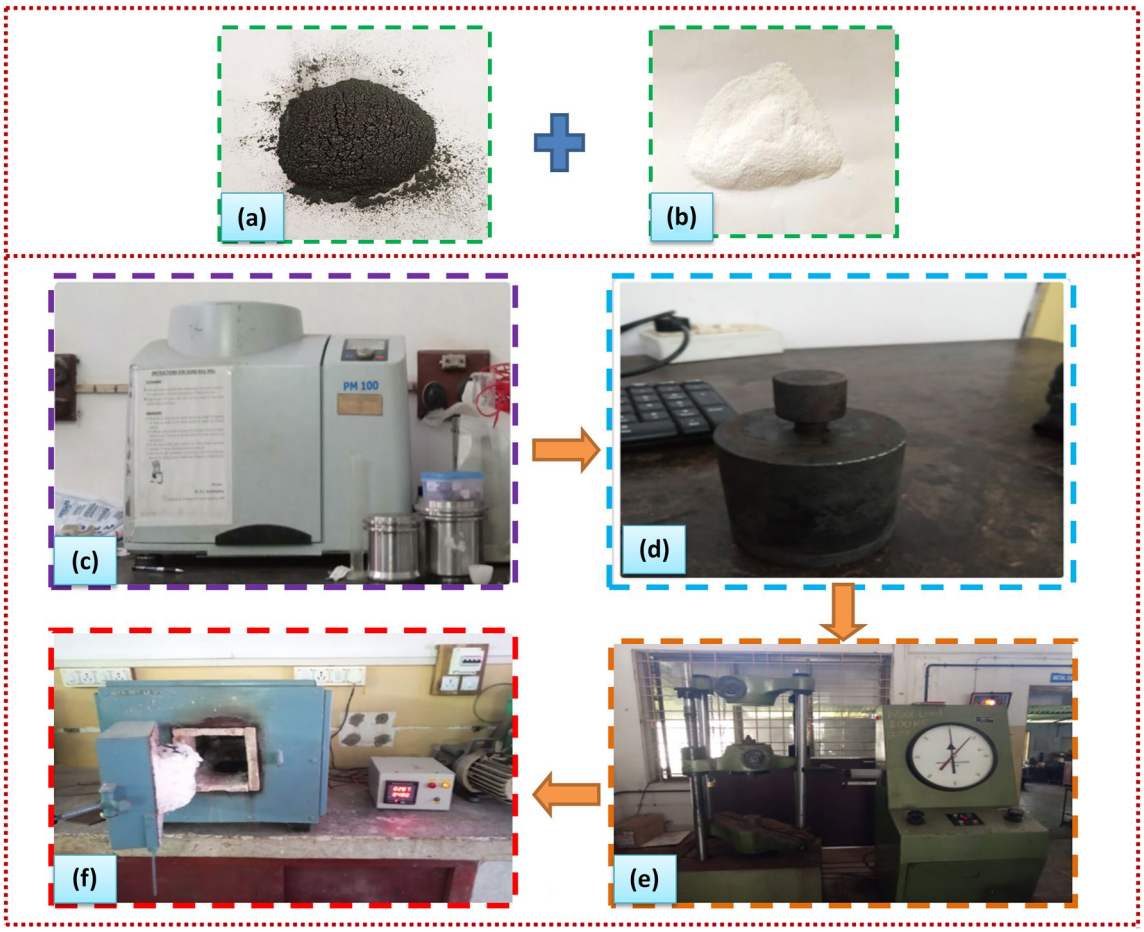

Fig. 3 **a** Aluminum (6061) powder **b** wax powder **c** high energy ball milling machine **d** die for compaction **e** UTM machine **f** electric resistance furnace

b); both powders are prepared in sufficient size using a ball milling machine as shown in Fig. 3c). The base powder AA6061 and wax foaming agent blended effectively with stirring speed 1000–1400 rpm up to 10 min. The specimens were compacted with a Die and UTM machine, as shown in Fig. 3d, e) by applying a 30 KN load so that both powders were closely packed with a cold compaction process. Then the samples were sintered for 30 min using an electric

furnace as shown in Fig. 3f). AA6061 metal powders supplied from M/s Metal Powder Company Ltd Tamil Nadu, India, were used as the base metal for producing metal foams. Foaming agent (wax powder supplied by LOBA Chemical, India). The literature study confirmed that the optimum proportion of foaming agent used in the powder metallurgy process to develop a foam is about 3–9%. As the foaming agent increases by more than 9% of the base material, the porosity increases, but the material's strength will decrease. So in the present work, the foaming agent as wax kept 3–9% of base powder (AA6061). During the stirring process, it separates into H2, leading to pores forming [36, 37, 44].

The morphology of the fabricated AMF was characterized by using the SEM. The phase structure of AFM is investigated using the X-ray diffraction method. Make- Bruker D8 Inc, Germany, with a source (λ Ʊ 1.5406 Å) Cu Kα radiation. The XRD pattern was recorded at a scanning rate of 1° per minute and 2θ range from 20° to 80° with a step size of 0.02°. The compressive tensile and flexural strength of all fabricated AMF specimens was investigated using a UTM per the ASTM standard [45].

The prepared specimens' density and percentage of porosity were measured using Archimedes' principle, as reported by Nawaz and Rani [31]. Density and porosity have been calculated as per the below equations.

The measured density and percentage of porosity of the prepared specimens are listed in Tables 1, Input process parameters and levels shown in Table 2.

$$\text{Density of foam} = \frac{\text{mass}}{\text{Volume of foam}} {}^{g}/_{cc} \quad (1)$$

$$\text{Porosity}(\%) = \frac{\text{The density of aluminium 6061} - \text{Density of foam in the specimen}}{\text{Density of aluminium 6061}} \times 100 \quad (2)$$

Table 2 Input process parameters along with their levels for the Taguchi approach

Input process parameters	Levels		
	1	2	3
A: Powder size (μm)	140	120	100
B: Stirring speed (rpm)	1400	1200	1000
C: Sintering temperature (°C)	500	400	300
D: Content of foaming agent (wt%) of base powder AA6061	3	6	9

2.2 Determination of mechanical properties of the prepared specimens

The mechanical properties like flexural, tensile, and compressive strengths have been determined using a computerized UTM with a speed of 2 mm/min and room temperature of 30 °C. The specimens before and after the test and the experimental details are shown in Figs. 4, 5, and 6. The measured mechanical properties are listed in Table 3. The mechanical properties determination is conducted as per the ISO and ASTM standards. The standard is ISO 13314-2011, with a specimen size of 30 mm cube to conduct compressive tests. The specimen before the compression test is shown in Fig. 4a) and the specimen position during the compression test is shown in Fig. 4b). The specimen after the compression test is shown in Fig. 4c). Compression test conducted as per the ISO 13314–2011 standard. This standard is used to determine the compressive strength of porous and cellular material with a porosity of more than 50% under the quasi-static strain rate condition at ambient temperature. The

Table 1 (%) porosity of the various AMF specimens

Specimen no	Initial vol. of water in measuring jar(MJ) in cc	Final vol. of water in measuring jar(MJ) in cc	Actual vol. of foam in cc	Mass of specimen in g	Density of foam in g/cc	Density of Aluminium (6061) in g/cc	Porosity (%)
1	500	566	66	58	0.88	2.7	67.45
2	500	568	68	60	0.88	2.7	67.32
3	500	570	70	62	0.89	2.7	67.20
4	500	576	76	61	0.80	2.7	70.27
5	500	583	83	65	0.78	2.7	71.00
6	500	593	93	73	0.78	2.7	70.93
7	500	581	81	65	0.80	2.7	70.28
8	500	589	89	70	0.79	2.7	70.87
9	500	602	102	79	0.77	2.7	71.31

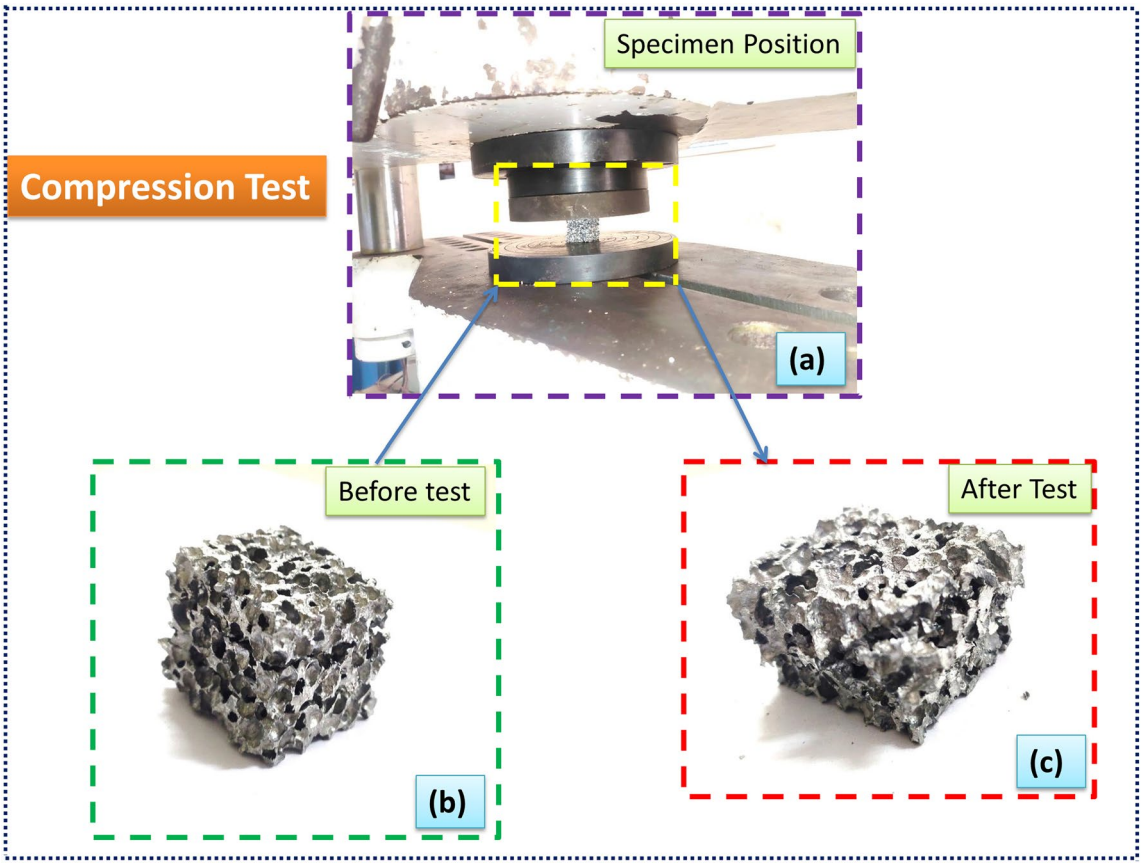

Fig. 4 **a** Compression test specimen of size: Cube 30 mm as per ISO 13314–2011, **b** compression test specimen position, **c** specimen after compression test

specimens are placed between the jaws at the UTM machine, and gradually compressive force is exerted until the specimen gets failure accordingly; the readings were recorded. The tensile test conducted per the standard uses ASTM D3039 with a specimen size of 200 mm × 25 mm × 12.5 mm. The specimen before the tensile test is shown in Fig. 5a), and the specimen's position during the tensile test is shown in Fig. 5b). The specimen after the tensile test is shown in Fig. 5c). During the tensile test, the specimen is placed in the gripper of UTM machine. The gradual tensile force was exerted until the specimen failed; the readings were recorded. The flexural test is conducted per the ASTM D790 standard with specimen size 110 mm × 30 mm × 10 mm with 3 point bending method. The specimen before the flexural test, as shown in Fig. 6a), the specimen position during the flexural test as shown in Fig. 6b), and the specimen after the flexural test, as shown in Fig. 6c). During the flexural test, the specimen is placed on the rollers of the bending fixture of UTM machine and gradually bending force exerted until the specimen gets failure accordingly the readings were recorded [46, 47].

2.3 Taguchi approach

Design of the experiment, Taguchi is the most famous statistical tool used to optimize the process for different parameters. It helps to minimize the number of experiments compared to the conventional experimental approach. This eventually helps to reduce the cost and time incurred in the traditional practical approach [40, 48]. The conventional experimental approach considers a single factor by changing one variable instantly, keeping others constant. The primary limitation of this conventional method is that it may exclude any possible interactions among the specified set of different parameters. The secondary drawback is that it will not be able to analyze the effect in a single experiment on all the factors and investigate their main effects. It has been observed that these limitations can be overcome by employing the Taguchi technique. The Taguchi approach estimates the output using the response function mean value for a defined parameter set. It also helps analyze and optimize the proper combinations in its input process parameters, giving the best output responses. The Taguchi approach will help transform the experimental data to signal a noise ratio. Various S/N ratios exist as per the required type

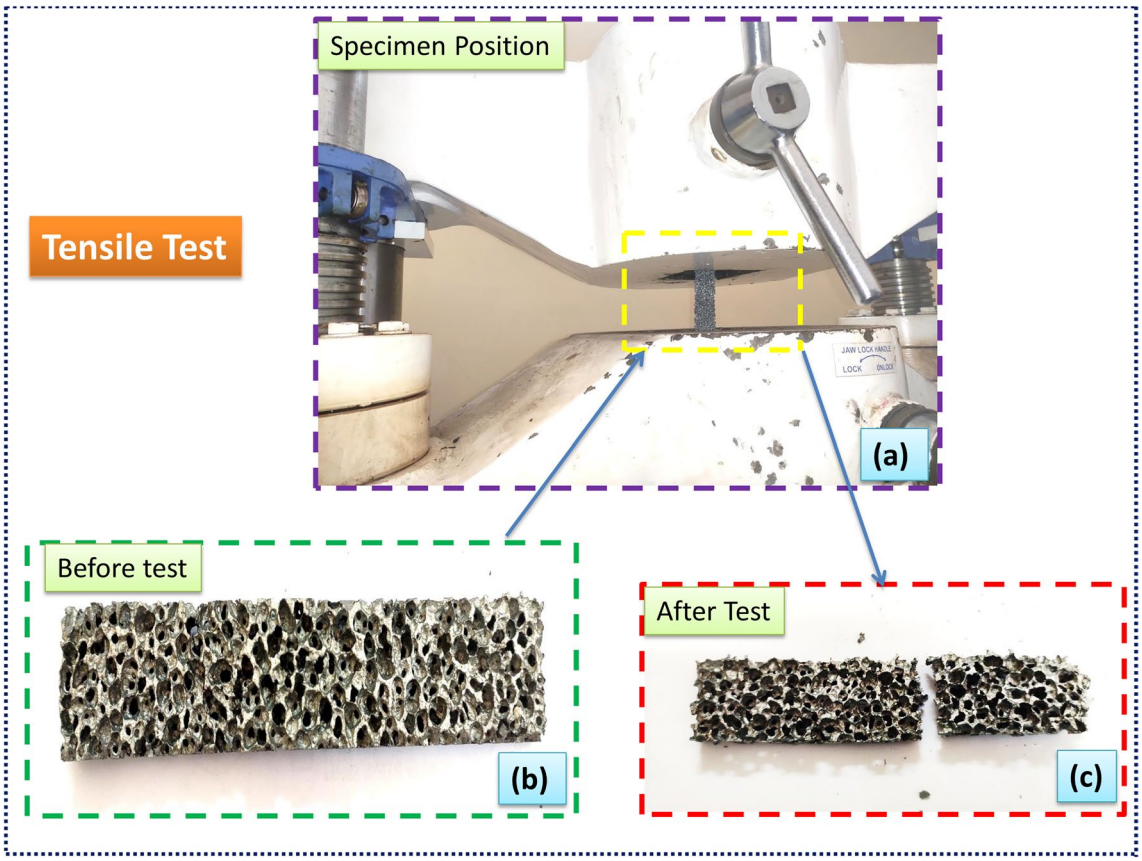

Fig. 5 **a** Tensile test specimen size: 200 mm × 25 mm × 12.5 mm, **b** tensile test specimen position, **c** specimen after tensile test

of its characteristics. The present work employs a significantly better signal-to-noised S/N ratio for all the output parameters. The S/N signal-to-noise ratio is evaluated with a logarithmic transformation of the loss function [40].

$$\frac{S}{N} = -10 \log \frac{1}{n}\left(y^2\right) \tag{3}$$

where y is the observed data & n is the total number of observations.

The four input process parameters used in the recent study, with their three.

The experimental runs were performed as mentioned in Table 3. The % contribution of the test parameters was investigated using the ANOVA technique. The mean and combined response characteristic curves are plotted using Minitab-17 software [40, 48].

3 Results and discussion

The morphological investigation of fabricated AMF (for sample 9 reported in Table 3) was performed using SEM and depicted in Fig. 7a, b). It shows that the homogeneous porous nature resulted from the dissolution of wax powder during the sintering process in the powder metallurgy technique.

The EDS analysis for the above-reported AMF sample is depicted in Fig. 8. The dark gray matrix phase is composed of (Al-Fe-Si). The other elemental compounds observed through EDS spectra are C, O, Mg, Ca, and Ti. The details of the EDS spectra value considered in weight and the atomic percentage are shown in Table 4.

An X-ray Diffraction (XRD) study shows the crystallographic phases within the prepared specimen (for sample 9 reported in Table 3). This XRD technique is carried out at room temperature, showing evidence that the prepared specimen with a foaming agent as a wax powder ($C_3H_6O_3$) shows the highest peak at 38 degrees, as shown in Fig. 9.

The effect of various input process parameters like powder size, sintering speed, sintering temperature, and foaming agent content on the mechanical properties of the developed AMF like porosity (%), compressive, tensile, and flexural strengths using the Taguchi DOE approach is discussed in below section.

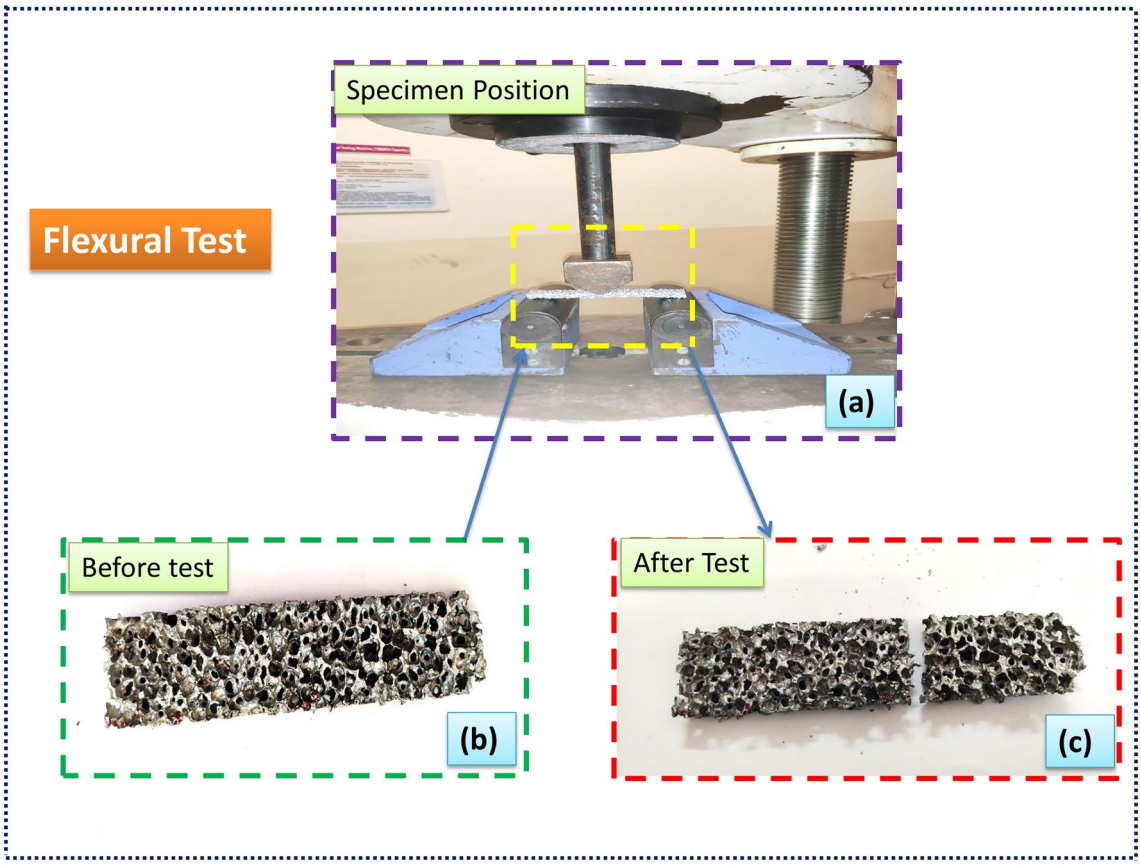

Fig. 6 **a** Flexural test specimen size: 110 mm × 30 mm × 10 mm, **b** flexural test specimen position, **c** specimen after flexural test

Table 3 Standard L9 orthogonal array for design of experiment

L9 exp. run	A powder size (μm)	B stirring speed (rpm)	C sintering temp (°C)	D Content of foaming agent (wt. %)	Porosity (%) porosity	Compressive strength (MPa)	Tensile strength (MPa)	Flexural strength (MPa)
1	140	1400	500	3	67.45	12.01	6.16	5.18
2	140	1200	400	6	67.32	11.51	5.17	4.82
3	140	1000	300	9	67.20	11.01	4.78	4.55
4	120	1400	400	9	70.27	10.51	4.48	5.05
5	120	1200	300	3	71.00	10.01	4.08	4.58
6	120	1000	500	6	70.93	9.51	3.98	4.48
7	100	1400	300	6	70.28	9.01	3.89	4.69
8	100	1200	500	9	70.87	8.51	3.81	3.90
9	100	1000	400	3	71.31	8.20	3.74	3.80

3.1 Effects of factors and ANOVA

3.1.1 Effects of process factors on porosity %

The data acquired using DOE L9 orthogonal array for output parameters, i.e., porosity (%), compressive, tensile, and flexural strengths, are transformed into S/N ratios listed in Tables 5, 6, 7, and 8, respectively. The significant factor's percentage (%) contribution is reported by ANOVA analysis for the respective output properties. The percentage contribution of significant factors on the % porosity is reported in ANOVA Table 5.

The ANOVA results showed that powder size significantly affects % porosity ($p = 74.14\%$), followed by

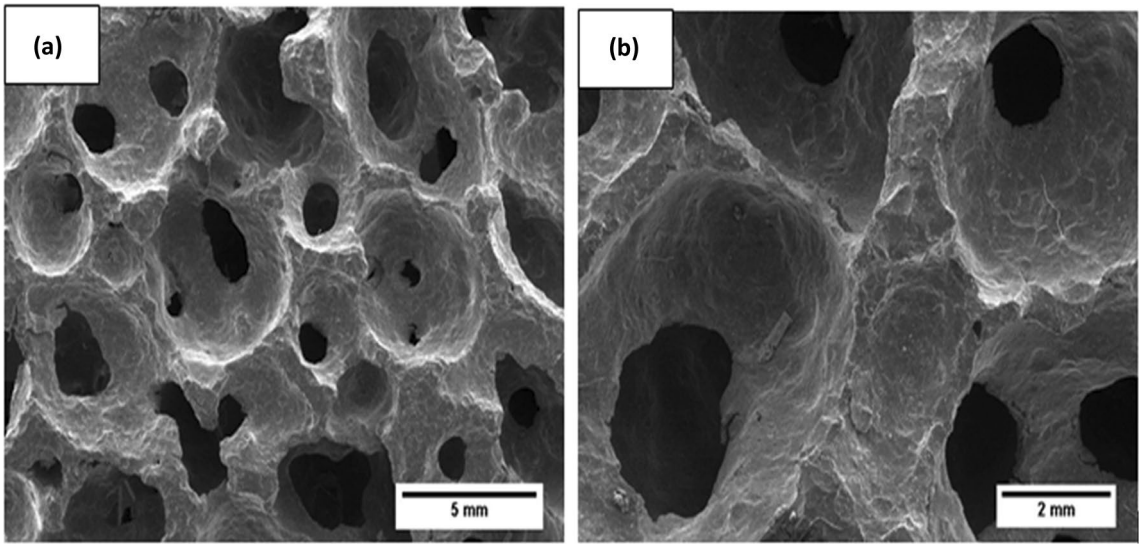

Fig. 7 Microstructure of AMF with different magnifications **a** 7X and **b** 20X showing the uniform network structure

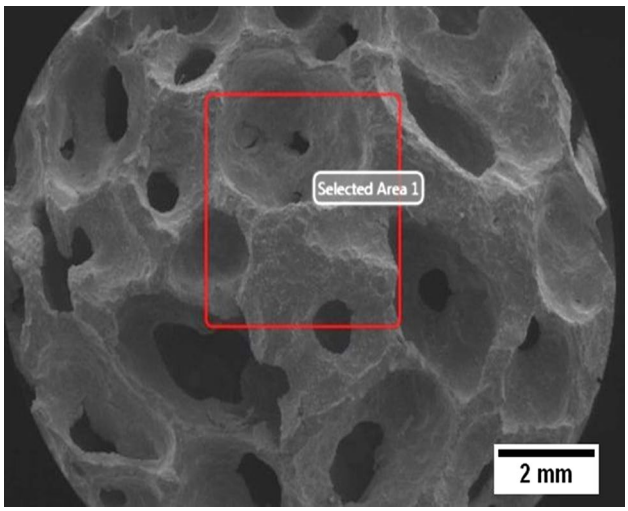

Fig. 8 EDS spectra for the fabricated AMF

Table 4 The elemental composition present in the AMF specimen

Element	Weight %	Atomic %
C	24.76	40.89
O	9.83	12.18
Mg	0.66	0.53
Al	60.04	44.13
Si	0.47	0.33
Ca	3.01	1.49
Ti	0.13	0.05
Fe	1.09	0.39

sintering speed ($p = 1.38\%$), wt. % of foaming agent ($p = 1.36\%$), and sintering temperature ($p = 0.41\%$) depicted minimum important and significant contributions to % porosity. The main and interaction plots depict individuals and affect their interaction on % porosity, as shown in Fig. 10.

The interaction plot for % porosity demonstrates that,

1. At higher powder sizes, the sintering speed has less influence on the % porosity, whereas at medium and lower powder sizes, as the sintering speed increases, the % porosity reduces.
2. At higher powder sizes, the sintering temperature has less influence on the % porosity. In the case of medium powder size, with an increase in sintering temperature, the % porosity decreases initially. It again increases due to the melting and bonding of the powder particles. In the case of lower powder size with an increase in sintering temperature, the % porosity decreases.
3. At higher powder sizes, the wt. % of foaming agent has less influence on the % porosity, whereas in the case of medium powder size with an increase in wt. % of foaming agent the % porosity decreases. Whereas in the case of lower powder size with an increase in wt. % of foaming agent, the % porosity decreases initially and increases again.

The maximum % porosity of 71.30 was observed with the combination of 100 µm powder size, 1000 rpm Stirring speed, 400 °C sintering temperature, and 3 wt. % of foaming agent.

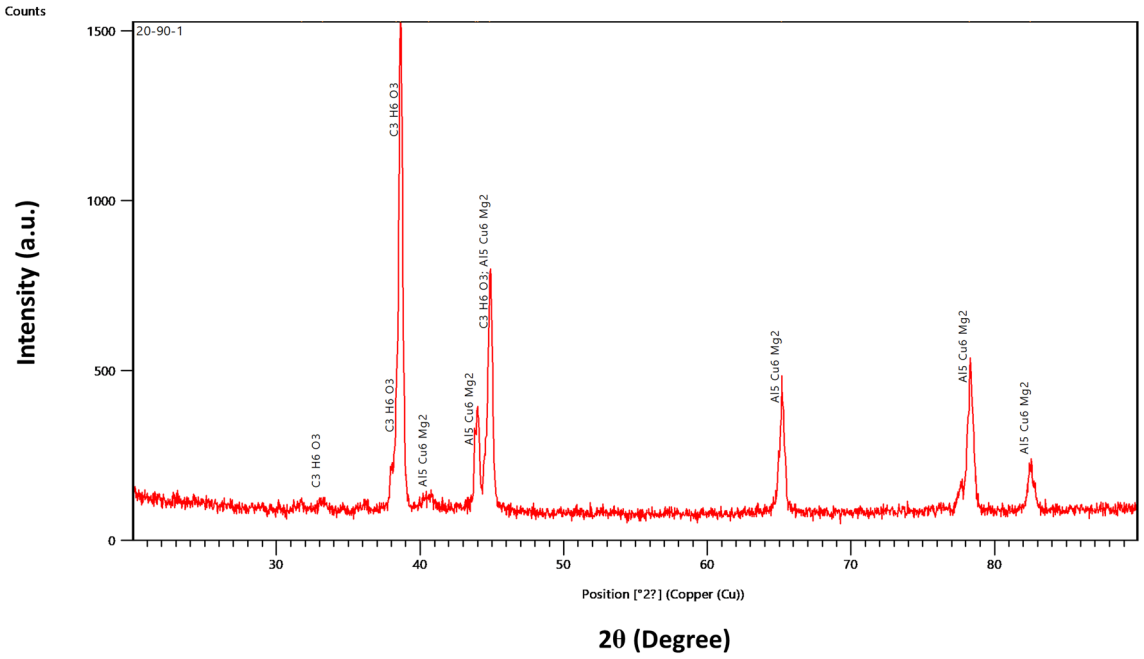

Fig. 9 X-ray diffraction pattern of AMF

Table 5 ANOVA results for porosity (%)

Source	DOF	Adj. SS	Adj. MS	F-Value	P Value	Percentage of contribution
A	1	18.3568	18.3568	13.06	0.022	74.14
B	1	0.3427	0.3427	0.24	0.647	1.38
C	1	0.1014	0.1014	0.07	0.801	0.41
D	1	0.3377	0.3377	0.24	0.650	1.36
Error	4	5.6208	1.4052			22.70
Total	8	24.7594				

Table 6 ANOVA results for compressive strength (MPa)

Source	DOF	Adj. SS	Adj. MS	F-Value	P Value	Percentage of contribution
A	1	16.6001	16.6001	113.27	0.000	85.02
B	1	1.6748	1.6748	11.43	0.028	8.58
C	1	0.1873	0.1873	1.28	0.321	2.44
D	1	0.4760	0.4760	3.25	0.146	0.96
Error	4	0.5862	0.1465			3.00
Total	8	19.5244				

3.1.2 Effects of process factors on compressive strength

The percentage contribution of significant factors to the compressive strength is reported in ANOVA Table 6. For compressive strength, it was observed that powder size has a significant influence ($p = 85.02\%$), followed by wt. % of foaming agent ($p = 81.20\%$), sintering speed ($p = 8.58\%$), and sintering temperature ($p = 0.96\%$) depicted the least significant contributions to compressive strength. The main plot and interaction plot depicts individuals and their interaction effects on compressive behavior, as shown in Fig. 11.

The interaction plot for compressive strength demonstrates that,

Table 7 ANOVA results for tensile strength (MPa)

Source	DOF	Adj. SS	Adj. MS	F Value	P Value	Percentage of contribution
A	1	3.6452	3.6452	33.16	0.005	70.69
B	1	0.6902	0.6902	6.28	0.066	13.38
C	1	0.2420	0.2420	2.20	0.212	4.69
D	1	0.1395	0.1395	1.27	0.323	2.70
Error	4	0.4397	0.1099			8.53
Total	8	5.1567				

Table 8 ANOVA results for flexural strength (MPa)

Source	DOF	Adj. SS	Adj. MS	F Value	P Value	Percentage of contribution
A	1	0.77533	0.775334	14.64	0.019	44.92
B	1	0.72659	0.726591	13.72	0.021	42.09
C	1	0.01168	0.011680	0.22	0.663	0.68
D	1	0.00061	0.000613	0.01	0.920	0.03
Error	4	0.21188	0.052970			12.27
Total	8	1.72610				

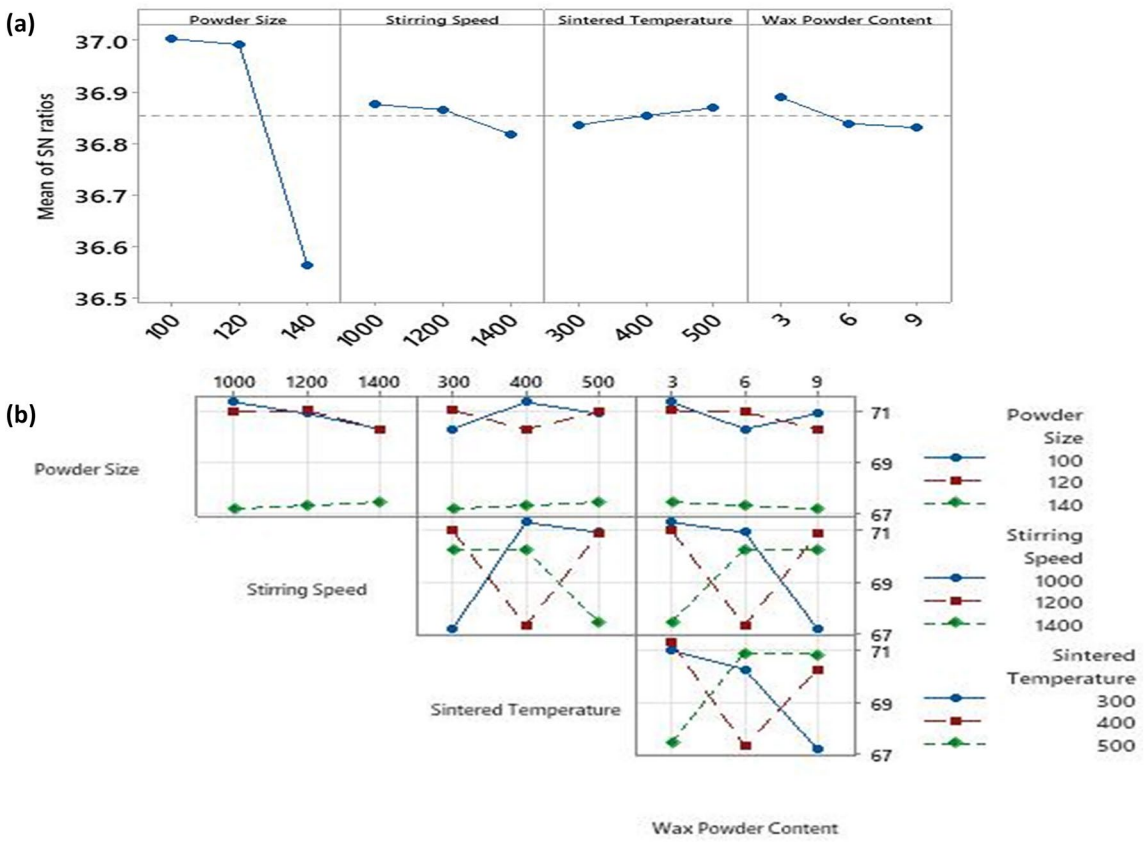

Fig. 10 % porosity **a** Main effect plot **b** Interaction plots for AMF sample

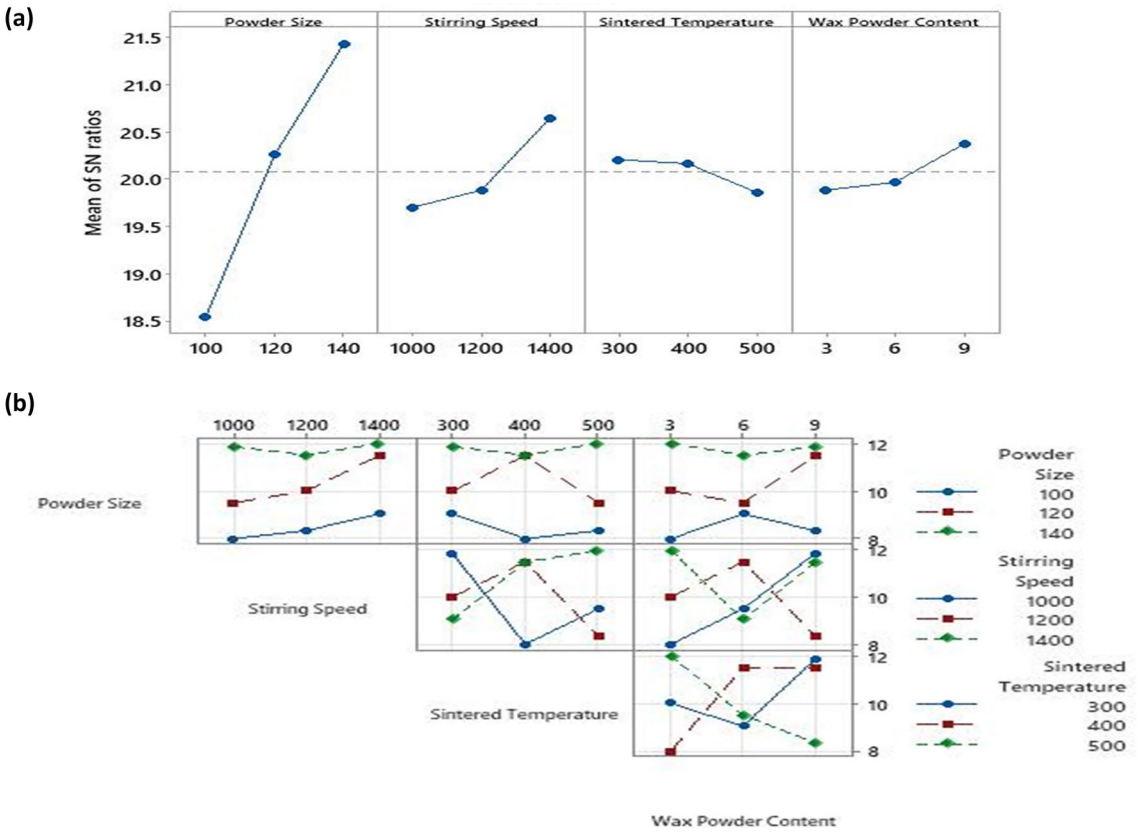

Fig. 11 Compressive strength **a** Main effect plot **b** Interaction plots for AMF sample

1. With the increase in powder size and sintering speed increase in the compressive strength is observed.
2. At lower powder sizes, with increasing in sintering temperature increase in the compressive strength is observed, whereas in the case of medium powder size, with an increase in sintering temperature reduction in the compressive strength is observed. Whereas in the case of higher powder size with an increase in sintering temperature increase in the compressive strength is observed.
3. At higher powder sizes, the wt. % of foaming agent has less influence on the compressive strength, whereas in the case of medium powder size with an increase in wt. % of foaming agent, the compressive strength increases. Whereas in the case of lower powder size with an increase in wt. % of foaming agent, the compressive strength increases initially and again goes on reducing.

The maximum compressive strength was observed with a combination of 140 µm powder size, 1400 rpm Stirring speed, 500 °C sintering temperature and 3 wt. % of foaming agent.

3.1.3 Effects of process factors on tensile strength

The % contribution of significant factors to the tensile strength is reported in ANOVA Table 7. For tensile strength, it was observed that powder size has the most significant influence ($p = 70.69\%$), afterwords by sintering speed ($p = 13.38\%$), sintering temperature ($p = 4.69\%$), and wt. % of foaming agent ($p = 2.70\%$) depicted least significant contributions to tensile strength. The main and interaction plots depict individuals and their effects on tensile strength, as shown in Fig. 12.

The interaction plot for tensile strength demonstrates that,

1. At lower and medium powder sizes, the sintering speed has less influence on the tensile strength, whereas at higher powder sizes, as the sintering speed increases, the tensile strength increases.
2. At lower powder sizes, the sintering temperature has less influence on the tensile strength, whereas in the case of medium powder size, with an increase in sintering temperature, the tensile strength increase initially and again goes on reducing. In the case of higher powder

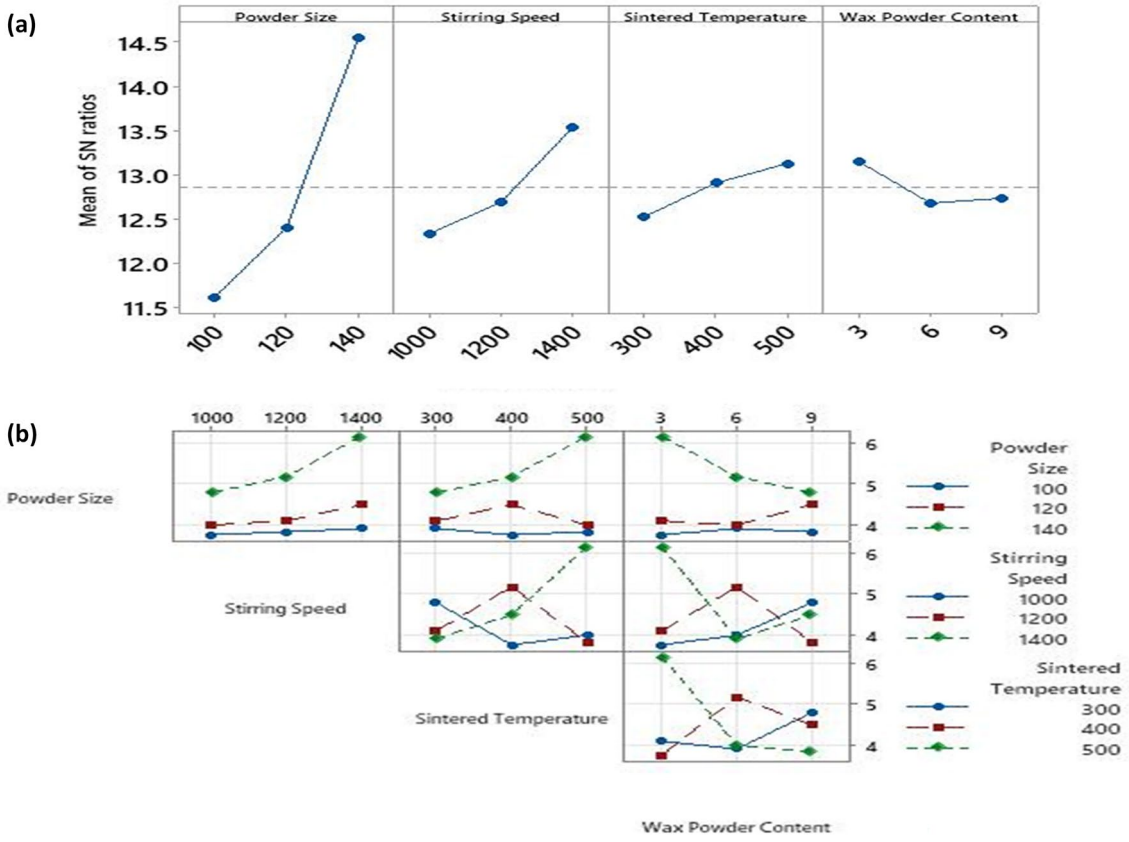

Fig. 12 Tensile strength **a** Main effect plot **b** Interaction plots for AMF sample

size with an increase in sintering temperature, increases in the tensile strength are observed.

3. At lower powder sizes, the wt. % of foaming agent has less influence on the tensile strength, whereas in the case of medium powder size with an increase in wt. % of foaming agent, the tensile strength increases. Whereas in the case of higher powder size with an increase in wt. % of foaming agent, the tensile strength decreases.

The maximum tensile strength was observed with a combination of 140 µm powder size, 1400 rpm Stirring speed, 500 °C sintering temperature and 3 wt. % of foaming agent.

3.1.4 Effects of process factors on flexural strength

The % contribution of significant factors to the flexural strength is reported in ANOVA Table 8. For flexural strength, it was observed that powder size has the highest influence ($p = 44.92\%$), afterword's by sintering speed ($p = 42.09\%$), sintering temperature ($p = 0.68\%$), and wt. % of foaming agent ($p = 0.03\%$) depicted the least significant contributions to flexural strength. The main and interaction plot depicts individuals and their effects on flexural strength, as shown in Fig. 13.

The interaction plot for flexural strength demonstrates that,

1. With the increase in powder size and sintering speed, an increase in flexural strength is observed.
2. At higher powder sizes with an increase in the sintering temperature, flexural strength increases, whereas in lower and medium powder sizes with an increase in sintering temperature, the flexural strength increases initially and again decreases.
3. At lower powder size with an increase in wt. % of foaming agent, the flexural strength increases initially and again goes on decreasing, whereas in the case of medium and higher powder size with an increase in wt. % of foaming agent, the flexural strength decreases.

The maximum tensile strength was observed with combination of 140 µm powder size, 1400 rpm Stirring speed, 500 °C sintering temperature and 3 wt. % of foaming agent.

3.2 Statistical interpretation using the Taguchi approach

In the present study, better criteria were applied for all the output properties of AMF to obtain an S/N ratio more

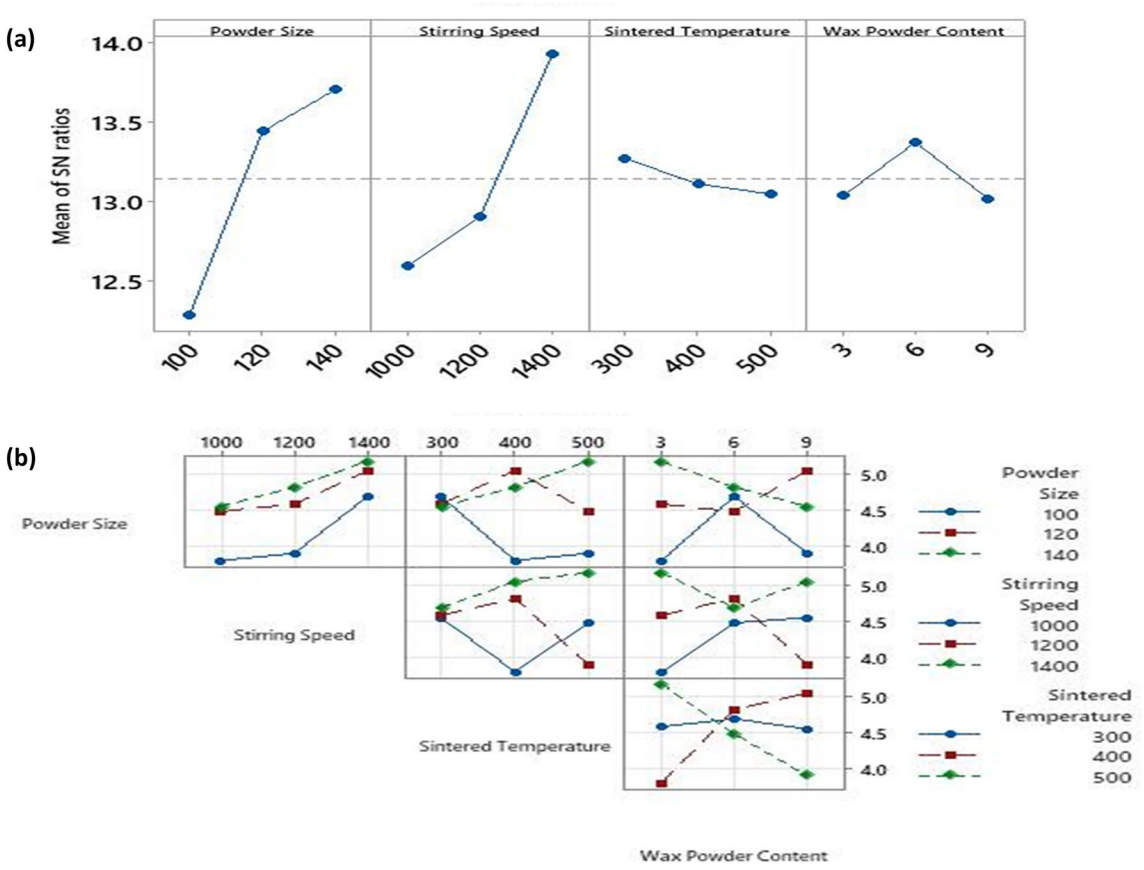

Fig. 13 Flexural strength **a** Main effect plot **b** Interaction plots for AMF sample

Table 9 Responses acquired in S/N ratios

% Porosity					Compressive strength (MPa)				
Level	A	B	C	D	Level	A	B	C	D
1	37.00	36.88	36.84	36.89	1	18.55	19.71	20.21	19.89
2	36.99	36.87	36.85	36.84	2	20.26	19.89	20.17	19.97
3	36.56	36.82	36.87	36.83	3	21.43	20.65	19.86	20.38
Delta	0.44	0.06	0.03	0.06	Delta	2.89	0.94	0.35	0.49
Rank	1	3	4	2	Rank	1	2	4	3
Tensile strength (MPa)					Flexural strength (MPa)				
Level	A	B	C	D	Level	A	B	C	D
1	11.61	12.34	12.52	13.15	1	12.28	12.59	13.27	13.03
2	12.40	12.69	12.91	12.68	2	13.44	12.90	13.11	13.37
3	14.55	13.53	13.13	12.73	3	13.70	13.92	13.04	13.02
Delta	2.93	1.19	0.61	0.47	Delta	1.42	1.33	0.23	0.35
Rank	1	2	3	4	Rank	1	2	4	3

significant. As per the considered criteria, the S/N signal-to-noise ratio should be higher to obtain optimum test conditions. The ranking for the input process factors is acquired using its S/N signal-to-noise ratios with four levels for % porosity and compressive, tensile, and flexural strength, as reported in Table 9. The ranks for the input process factors are obtained to establish the relative magnitude of effects based on the delta statistics [36].

Table 10 Confirmation tests

	Initial parameter combination	Prediction	Experimentation	Improvement in S/N ratio
Level	A1B1C1D1	A1B1C3D1		
% porosity	67.45	67.74	69.91	
SN ratio (dB)	36.57	36.72	37.89	3.20
Level	A3B3C2D1	A3B3C2D3		
Compressive strength (MPa)	8.20	8.29	7.89	
SN ratio (dB)	18.22	18.43	17.54	5.99
Level	A3B3C2D1	A3B3C1D1		
Tensile strength (MPa)	3.74	3.68	4.02	
SN ratio (dB)	11.44	11.25	12.28	9.23
Level	A3B3C2D1	A3B3C1D2		
Flexural strength (MPa)	3.80	3.81	3.94	
SN ratio (dB)	11.59	11.62	12.01	3.35

3.3 Confirmation tests

In the DOE approach, the final step is the confirmation of experiments. After investigating the optimal test conditions, the confirmation was performed considering the optimum level of factors. The acquired results were eventually compared with the predicted results [40]. Table 10 demonstrates the comparative results obtained using optimal parameters. It has been observed that there was reasonable agreement between the experimental and predicted results. However, an error of 3.20% for % porosity, 5.99% compressive strength, 9.23% tensile strength, and 3.35% flexural strength (S/N ratios) was observed.

4 Conclusion

The mechanical properties of the developed AMF with various influential parameters such as powder size, sintering speed, sintering temperature, and foaming agent content have been studied. Furthermore, Taguchi's design of the experiment and ANOVA were performed to have a good correlation between the listed input and output parameters. Based on experimental and DOE approaches, the conclusions below have been drawn.

1. These experimental test results show that the powder metallurgy approach helps produce lightweight Aluminium metal foam (AMF) with a uniform homogeneous structure using wax powder as a foaming agent.
2. The maximum porosity is 71.30%, Compression strength 12.01 MPa, Tensile strength is 6.16 MPa, and Flexural strength is 5.18 MPa. The microstructure study reveals that there is no adequate composition in the specimen.
3. Taguchi's approach reveals that powder size is the most influential parameter, followed by stirring speed, wt. % of foaming agent and sintering temperature affecting the output mechanical properties. Among all, sintering temperature effects as less individually, but as in the case of a combined interaction effect, it affects significantly.
4. Research works concludes that powder metallurgy is the best technique to develop metal foam with a foaming agent as paraffin wax powder. It gives the solution to the most challenging task of producing metal foam with uniform integrity on entire surfaces with good mechanical properties.

Supplementary Information The online version of this article contains supplementary material available https://doi.org/10.1007/s10934-022-01405-z.

Author contributions Mr. MM: Experimental work about producing metal foam through powder metallurgy technique and literature study about the topic. Dr. SCG: Drafting the journal paper as per the format and checking the grammatical mistakes. Dr. AVB: Implementing the Design of experiments with the Taguchi approach.

Funding The author(s) received no financial support for this article's research, authorship and publication.

Declarations

Conflict of interest The author(s) declared no potential conflicts of interest with respect to the research, authorship, and/or publication of this article.

References

1. D.K. Rajak, L.A. Kumaraswamidhas, S. Das, Rev. Adv. Mater. Sci. **49**, 68–86 (2017)
2. A.V. Borgaonkar, V.G. Salunkhe, M.B. Kumbhar, A.R. Koli, S.B. Potdar, Mater. Today: Proc. **38**, 2222–2226 (2021)

3. S. Singh, N. Bhatnagar, J. Porous Mater. **25**, 537–554 (2018)
4. A.V. Borgaonkar, M.B. Mandale, S.B. Potdar, Mater. Today: Proc **5**, 5356–5364 (2018)
5. A.V. Borgaonkar, S.B. Potdar, *Tribology of polymer and polymer composite for industry 4.0* (Springer, Singapore, 2021), pp.1–13
6. A. Kulshreshtha, S.K. Dhakad, Mater. Today: Proc **26**, 1784–1790 (2020)
7. A.V. Borgaonkar, M.B. Mandale Salunkhe, V.G. Potdar, Mater. Today: Proc. **26**, 256–260 (2020)
8. P. Patel, P. Bhingole, D. Makwana, Mater. Today: Proc. **5**, 20391–20402 (2018)
9. B. Bauer, S. Kralj, M. Bušić, Tech. Gaz. **20**, 1095–1102 (2013)
10. N. Babcsan, S. Beke, P. Makk, G. Szamel, C. Kadar, Procedia Mater. Sci. **4**, 127–132 (2014)
11. H. Bafti, A. Habibolahzadeh, Mater. Des. **52**, 404–411 (2013)
12. O. Gîngu, G. Sima, C. Teișanu, I.G. Bucşe, Appl. Mech. Mater. **880**, 248–255 (2018)
13. Z. Li, C. Xi, L. Jing, Z. Wang, L. Zhao, Mater. Sci. Eng. **592**, 221–229 (2014)
14. A. Güner, M. Arıkan, M. Nebioglu, Metals **5**, 1553–1565 (2015)
15. T. Shimizu, K. Matsuzaki, J. Jpn. Soc. Powder Metall. **50**, 177–181 (2003)
16. D.K. Rajak, M. Gupta, *In an insight into metal based foams* (Springer, Singapore, 2020), pp.39–52
17. F. García-Moreno, Materials. **9**(2), 85 (2016)
18. A. Borgaonkar, M.B. Mandale, C.S. Chaitanya, S.B. Potdar, *Recent advances in layered materials and structures* (Springer, Singapore, 2021), pp.307–330
19. B.A. Bouwhuis, J. McCrea, G. Palumbo, G.D. Hibbard, Acta Mater. **57**, 4046–4053 (2009)
20. J.A. Brown, L.J. Vendra, A. Rabiei, Metall. Mater. Trans. **41**, 2784–2793 (2010)
21. N. Dukhan, N. Rayess, J. Hadley, Mech. Mater. **42**, 134–141 (2010)
22. G. D'Urso, G. Maccarini, Int. J. Mater. Form. **5**, 243–257 (2012)
23. A. Kim, M.A. Hasan, S.H. Nahm, S.S. Cho, Compos. Struct. **71**, 191–198 (2005)
24. J. Kadkhodapour, S. Raeisi, Comput. Mater. Sci. **83**, 137–148 (2014)
25. A. Jung, S. Diebels, Adv. Eng. Mater. **21**, 1900237 (2019)
26. A. Jung, S. Diebels, Eur J. Eng. Mech. **34**, 12–22 (2014)
27. A. Jung, M. Wocker, Z. Chen, H. Seibert, Mater. Des. **88**, 1021–1030 (2015)
28. I. Duarte, J.M. Ferreira, Materials **9**(2), 79 (2016)
29. I.N. Orbulov, A. Szlancsik, Adv. Eng. Mater. **20**, 1700980 (2018)
30. V.C. Shunmugasamy, B. Mansoor, Mater. Sci. Eng. A **715**, 281–294 (2018)
31. A. Nawaz, S. Rani, Mater. Today: Proc. **47**, 6025–6029 (2021)
32. P.S. Liu, Philos. Mag. Lett. **90**, 447–453 (2010)
33. X.Z. Wang, L. Wu, S.X. Wang, Mater. Technol. **24**, 161–165 (2009)
34. A. Uzun, H. Karakoc, U. Gokmen, H. Cinici, M. Turker, Int. J. Mater. Res. **107**, 996–1004 (2016)
35. T. Shi, X. Chen, Y. Cheng, Y. Liu, H. Zhang, Y. Li **59**, 625–633 (2018)
36. M.A. Naeem, A. Gábora, T. Mankovits. Influence of the manufacturing parameters on the compressive properties of closed cell aluminum foams. Period. Polytech. Mech. Eng. **64**, 172–178 (2020)
37. M. Mahadev, C.G. Sreenivasa, K.M. Shivakumar, IOP Conf. Ser. Mater. Sci. Eng. **376**, 1–12 (2018)
38. E. Solórzano, J.A. Reglero, M.A. Rodríguez-Pérez, J.A. de Saja, M.L. Rodríguez-Méndez, J. Mater. Sci. **42**, 7227–7238 (2007)
39. R. Surace, S. Bruno, L.A. De Filippis, A.D. Ludovico, Int. J. Simul. Model. **8**, 81–89 (2009)
40. A. Borgaonkar, I. Syed, Proc. Inst. Mech. Eng. C: J. Mech **0**, 1–16 (2021)
41. A. Uzun, Compos. B. Eng. **172**, 206–217 (2019)
42. X. Ding, Y. Liu, X. Chen, H. Zhang, Y. Li, Mater. Lett. **216**, 38–41 (2018)
43. T. Geramipour, H. Oveisi, Trans. Nonferrous Met. Soc. China **27**, 1569–1579 (2017)
44. H. Ali, A. Gábora, M.A. Naeem, G. Kalácska, T. Mankovits, Int. J. Appl. Sci. **12**, 230–237 (2021)
45. M. Madgule, C.G. Sreenivasa, G.C. Manjunath Patel, L. Avinash, S. Piyush, P. Dhiren, V. Malik, Part E: J. Process Mech. Eng. **0**, 1–13 (2022)
46. M. Mahadev, C.G. Sreenivasa, J. Optoelectron. Laser **41**, 655–662 (2022)
47. M.J. Mirzaali, F. Libonati, P. Vena, V. Mussi, L. Vergani, M. Strano, Procedia Struct. Integr. **2**, 1285–1294 (2016)
48. S.B. Potdar, B.A. Bhanvase, P. Saudagar, I. Potoroko, S.H. Sonawane, Can. J. Chem. Eng. **100**, 1718–1728 (2022)